Holographic codes seen through ZX-calculus (arXiv:2601.04467)

Kwok Ho Wan,[1,2] Henry C. W. Price,[3] and Qing Yao[3,4]

[1] *Blackett Laboratory, Imperial College London, London SW7 2AZ, UK*
[2] *Mathematical Institute, University of Oxford, Woodstock Road, Oxford OX2 6GG, UK*
[3] *Centre for Complexity Science, Imperial College London, London SW7 2AZ, UK*
[4] *Mailman School of Public Health, Columbia University, New York, NY, USA.*

(Dated: February 22, 2026)

I. INTRODUCTION

Holographic tensor networks provide a concrete bridge between ideas from AdS/CFT and quantum error correction: bulk degrees of freedom can be redundantly encoded into boundary degrees of freedom, and erasures on the boundary can be interpreted as correctable noise [1, 2]. The pentagon holographic code [2] is a prominent example, built from six-qubit perfect tensors arranged on a $\{5, 4\}$ hyperbolic tessellation.

Most analyses of such codes proceed in the tensor-network language, where geometry suggests entanglement structure and decoding is phrased in terms of operator pushing and greedy algorithms [2, 3]. In this work we advocate a complementary viewpoint: for stabiliser codes, ZX-calculus provides a graphical language in which (i) tensor identities become diagrammatic equalities, and (ii) stabilisers and logical operators can be represented and manipulated as Pauli webs. Once a holographic encoder is expressed as a Clifford ZX-diagram, one can algorithmically extract stabiliser generators, parity check matrices, and boundary representatives of bulk logical operators using standard ZX tooling [4–6].

We re-visit the pentagon holographic code through ZX-calculus and Pauli webs, provide numerical simulations of isometry-defined codes based on generalisations of its ZX-diagram construction, study logical performance under belief propagation (BP) decoders [7], and illustrate how generator choices and gauge-fixing prescriptions can dramatically affect decoder performance (in line with [3]).

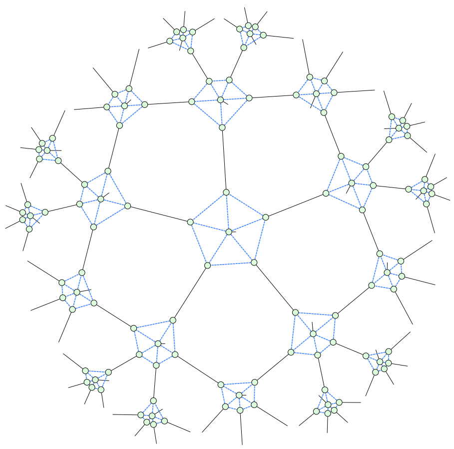
$$\longleftrightarrow$$
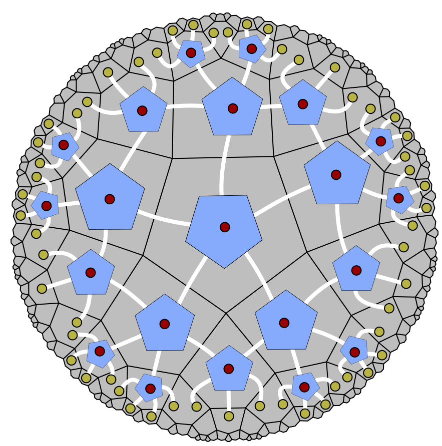
(1)

II. ZX-DIAGRAMS AND THE PENTAGON HOLOGRAPHIC CODE

ZX-diagrams [8] provide a diagrammatic language for tensors built from three primitives: Z-spiders, X-spiders, and Hadamard boxes. The m-legged Z-spider with phase α is the tensor $e^{i\,\delta_{1,i_1}\alpha}\,\delta_{i_1,\ldots,i_m}$, corresponding to the (unnormalised) state $|0\rangle^{\otimes m} + e^{i\alpha}\,|1\rangle^{\otimes m}$. The X-spider is obtained by contracting each leg of a Z-spider with a Hadamard. Equipped with rewrite rules that preserve the represented linear map, ZX-diagrams support compositional reasoning about quantum states and processes.

The six-qubit perfect tensor underpinning the pentagon code admits a natural ZX-diagram realisation as a graph state (up to a local Hadamard on the bulk qubit leg) [9]. Its stabiliser group comprises the four generators of the $[[5, 1, 3]]$ code and two generators coupling the bulk qubit to the logical operators:

$$\begin{aligned}\big\langle\; & XZZXI \otimes I,\; IXZZX \otimes I, \\ & XIXZZ \otimes I,\; ZXIXZ \otimes I, \\ & \underbrace{XXXXX}_{\bar{X}_{[[5,1,3]]}} \otimes X,\; \underbrace{ZZZZZ}_{\bar{Z}_{[[5,1,3]]}} \otimes Z \;\big\rangle\,.\end{aligned} \tag{2}$$

Tiling the $\{5, 4\}$ hyperbolic tessellation with these graph-state chunks and contracting shared legs produces the full pentagon holographic code as a single ZX-diagram (equation 1). The encoding rate satisfies $N_{\text{bulk}}/N_{\text{boundary}} \to 1/\sqrt{5}$ as $n \to \infty$, which we verify numerically. Since the ZX-diagram is phase-less and only connectivity matters [8], it can be interpreted interchangeably as the encoding isometry V, its adjoint $V^\dagger$, or a collection of logical Bell pairs between bulk and boundary qubits.

III. STABILISERS, LOGICAL OPERATORS, AND ERASURE DECODING

Pauli webs [6] are graphical annotations on ZX-diagrams that track the propagation of Pauli operators through Clifford constructions. A stabiliser of the code corresponds to a Pauli web supported only on boundary legs, satisfying $S_\partial V = V$. A logical operator corresponds to a web with additional support on a bulk leg, giving a boundary representative L_∂ such that $L_\partial V = V \bar{L}$. Reading off the Pauli colouring on boundary legs and converting to binary symplectic form yields rows of the parity-check matrix [10]. Using generated Pauli webs, we construct the parity-check matrix and reproduce the erasure-decoding results of [2] with a peeling decoder [11], matching the shape of the original greedy-decoder curves.

IV. THE $\{4,5\}$ ZX-HOLOGRAPHIC CODE FAMILY

Motivated by the pentagon code's ZX structure on $\{p,q\} = \{5,4\}$, we introduce a family of codes on the dual tessellation $\{p,q\} = \{4,5\}$ [12]. Each tensor vertex is replaced by a specific 5-qubit ZX-diagram whose stabilisers closely mirror those of the $[[4,1,2]]$ encoder: $\langle ZZYY \otimes I,\ XIXI \otimes I,\ IXIX \otimes I,\ ZIZX \otimes Z,\ IIXX \otimes X\rangle$. Iterating over tessellation layers generates codes of increasing size:

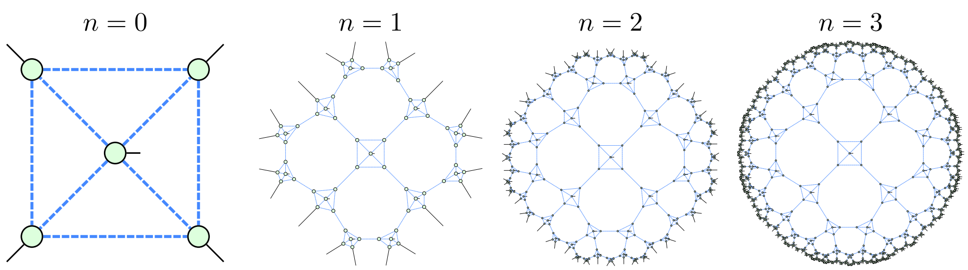

$$\cdots \tag{3}$$

We extract quantum codes by computing Pauli webs supported exclusively on the boundary qubits and study the logical error rate of the central bulk qubit under erasure and depolarising noise.

A. Erasure decoding

We consider an erasure noise model on boundary qubits, each erased independently with probability p. Without gauge fixing, no erasure threshold is observed as n increases. Following a gauge-fixing prescription, we project all bulk qubits except the central one onto fixed eigenstates. Fixing to $|0\rangle^{\otimes(N_{\text{bulk}}-1)}$ (Z-eigenstates) yields no threshold. In contrast, projecting onto $|+\rangle^{\otimes(N_{\text{bulk}}-1)}$ (X-eigenstates) with BP+OSD-0 decoding achieves a near-optimal threshold at $\approx \frac{1}{2}$ erasure rate (figure 1). The effective code distance grows rapidly with n:

n	fit ($\approx p_{\text{L}}$)	distance ($\approx d$)	N_{boundary}
0	$2 \times p_e^2$	2	4
1	$10 \times p_e^4$	4	20
2	$20 \times p_e^6$	6	76
3	$5 \times 10^4 \times p_e^{16}$	16	284
4	$10^9 \times p_e^{30}$	30	1060

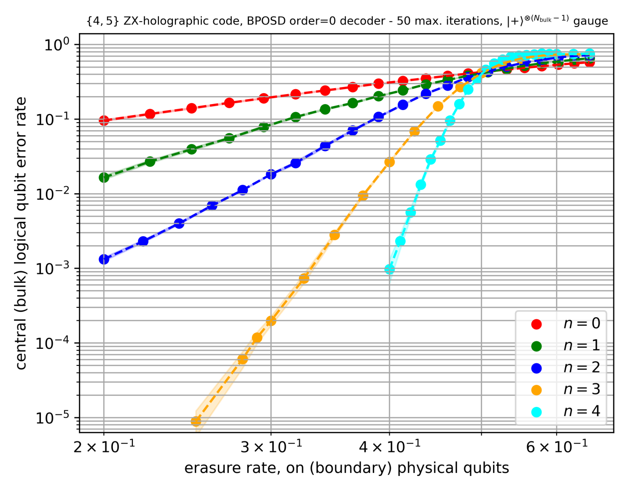

Figure 1. Logical error rate of the central bulk qubit for $|+\rangle^{\otimes(N_{\text{bulk}}-1)}$ gauge fixing, decoded using BP+OSD−0, under erasure errors at the boundary.

B. Pauli error decoding

Under depolarising noise ($\rho \to (1-p)\rho + \frac{p}{3}(X\rho X + Y\rho Y + Z\rho Z)$ on each boundary qubit), BP alone fails to show threshold-like behaviour for larger n. Inspection of the parity-check matrix $H \in \mathbb{F}_2^{m \times 2N_{\text{boundary}}}$ reveals heavy-tailed check weights and large overlaps that degrade BP. We introduce a smoothing heuristic based on elementary row operations over $\mathbb{F}_2$: iteratively selecting the heaviest check row and XOR-combining it with candidates to reduce Hamming weight ($H_i \leftarrow H_i \oplus H_j$). Combined with BP+OSD (order = 10), this yields improved logical error suppression (figure 2), confirming that the observed performance is largely decoder-limited.

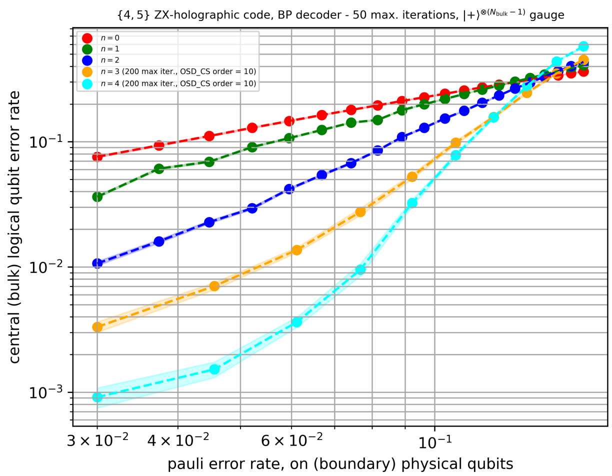

Figure 2. Logical error rate of the central bulk qubit for $|+\rangle^{\otimes(N_{\text{bulk}}-1)}$ gauge fixing, decoded using BP (for $n = 0, 1, 2$) and BP+OSD (for $n = 3, 4$), under random Pauli depolarising errors at the boundary with heuristic row operations that reduce stabiliser weight.

C. Erasure vs Pauli noise error-suppression region

Interpolating between pure erasure (rate p_e) and pure depolarising noise (rate p_r), we map out a two-dimensional error-suppression region in the (p_e, p_r) plane where larger codes outperform smaller ones (figure 3). This finite-size, decoder-dependent region serves as a useful diagnostic of the code's noise tolerance.

V. SUMMARY AND OUTLOOK

We have demonstrated the utility of ZX-calculus and Pauli webs for analysing stabiliser holographic codes. The framework provides automated extraction of stabilisers, logical operators, and parity-check matrices from ZX-diagram encoders, as well as diagrammatic computation of Rényi entropies and transparent representations of toy black-hole and wormhole constructions. Building on this, we introduced the $\{4, 5\}$ ZX-holographic code family and showed that gauge-fixing prescriptions, generator choices, and decoder selection critically affect logical error rates. With X-gauge fixing and BP+OSD decoding, the codes exhibit rapidly growing effective distance under erasure noise and a near-optimal erasure threshold of $\approx \frac{1}{2}$. These results suggest that ZX-diagrammatically motivated tensor networks are a useful design tool towards interesting holographic and tensor network codes.

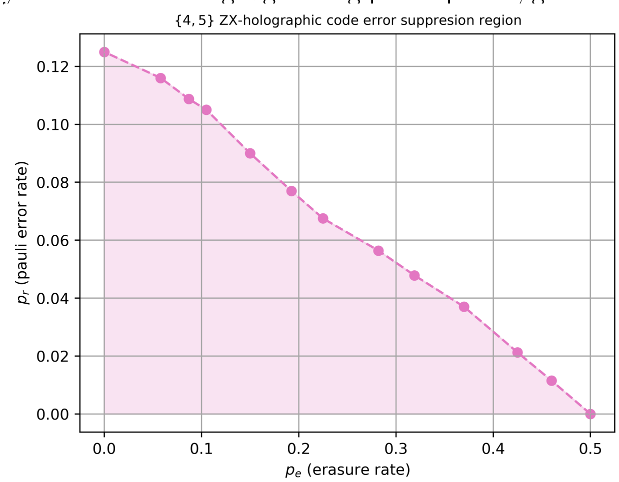

Figure 3. Error suppression region of the central bulk qubit in the (p_e, p_r) plane. $|+\rangle^{\otimes(N_{\text{bulk}}-1)}$ gauge fixing, decoded using BP+OSD with order = 10 and 200 maximum iterations. Heuristic row operations were also used.

[1] A. Almheiri, X. Dong, and D. Harlow, JHEP **04**, 163, arXiv:1411.7041 [hep-th].

[2] F. Pastawski, B. Yoshida, D. Harlow, and J. Preskill, JHEP **06**, 149, arXiv:1503.06237 [hep-th].

[3] M. Steinberg, J. Fan, R. J. Harris, D. Elkouss, S. Feld, and A. Jahn, Quantum **9**, 1826 (2025).

[4] A. Kissinger and J. van de Wetering, in *Proceedings 16th International Conference on Quantum Physics and Logic, Chapman University, Orange, CA, USA., 10-14 June 2019*, Electronic Proceedings in Theoretical Computer Science, Vol. 318, edited by B. Coecke and M. Leifer (Open Publishing Association, 2020) pp. 229–241.

[5] M. Rüsch, B. Rodatz, and A. Kissinger, Completeness for fault equivalence of clifford zx diagrams (2025), arXiv:2510.08477 [quant-ph].

[6] H. Bombin, D. Litinski, N. Nickerson, F. Pastawski, and S. Roberts, Quantum **8**, 1379 (2024).

[7] J. Roffe, LDPC: Python tools for low density parity check codes (2022).

[8] A. Kissinger and J. van de Wetering, *Picturing Quantum Software: An Introduction to the ZX-Calculus and Quantum Compilation* (Preprint, 2024).

[9] Z. Wu, S. Cheng, and B. Zeng, A ZX-calculus approach for the construction of graph codes (2024), arXiv:2304.08363 [quant-ph].

[10] D. Gottesman, The Heisenberg Representation of Quantum Computers (1998), arXiv:quant-ph/9807006 [quant-ph].

[11] N. Connolly, V. Londe, A. Leverrier, and N. Delfosse, Quantum **8**, 1450 (2024).

[12] D. A. Jahn, Holographic codes and critical lattice theories (2023), youTube video.